Int. J. Appl. Ceram. Technol., 12 [5] 1016–1019 (2015)
DOI:10.1111/ijac.12312

Structural and Spectroscopic Properties of δ-$Y_2Si_2O_7$ Nanopowders Activated with Nd^{3+} Ions

Murat Erdem*

Department of Physics, Marmara University, 34722 Istanbul, Turkey

Department of Physics, Boston College, Chestnut Hill, Massachusetts, 02467

Mete Kaan Ekmekci

Department of Chemistry, Marmara University, 34722 Istanbul, Turkey

Humeyra Orucu

Department of Physics, Ege University, 35100 Izmir, Turkey

Gokhan Bilir

Department of Physics, Boston College, Chestnut Hill, Massachusetts, 02467

Department of Physics Engineering, Istanbul Technical University, 34469 Istanbul, Turkey

Phosphors of δ-$Y_2Si_2O_7$ doped with Nd^{3+} ions were prepared in the SiO_2–Y_2O_3 binary systems using the solgel technique. Nano-sized crystalline phosphor powders were obtained by annealing the dried gels at 1480°C. The average grain sizes of the NYS1, NYS2, NYS3, and NYS4, powders were estimated to be 44.1, 41.3, 48.1, and 53.2 nm from the grain size distribution curves, respectively, and these results were confirmed by transmission electron microscope measurements. The spectroscopic properties of the powders were studied by measuring the luminescence spectra, and the decay curves of the $^4F_{3/2}$ emission level were measured at room temperature.

Introduction

The nanomaterials doped with optically active ions attracted considerable attention, and most of the studies in the literature devoted to the fabrication and characterization of these materials due to their potential application in photonics and optoelectronics. This interest on such host materials steadily increased with the development of new and cheap synthetic methods.

Yttrium silicate (Y_2SiO_5, $Y_2Si_2O_7$) ceramic powders doped with rare earth ions have found applications in the preparation of efficient laser ceramics, optical memory devices, and high energy phosphors.[1–5] The host lattice of yttrium disilicate ($Y_2Si_2O_7$) shows high luminescence quantum efficiency as well as excellent chemical and thermal property.[5,6] It has been shown in the literature that the structural phases due to its complex high-temperature polymorphism are in the *y*, z, α, β, γ, and δ forms.[7] Therefore, the main goal of the recent study was to prepare ceramic as a single-phase material.

δ-$Y_2Si_2O_7$ crystallizes into an orthorhombic structure with the $Pna2_1$ space group and assigns unique crystallographic site to Y^{3+} ions both with seven coordination number.[8] The insulating host materials doped with Nd^{3+} ions offer the possibility of UV, visible, and IR emission channels according to a four-level scheme by direct excitation or by an up-conversion mechanism.[9,10]

To the best of our knowledge, a few papers have been devoted to the study of un-doped δ-$Y_2Si_2O_7$ in the literature,[11–13] but there is no study available about the Nd^{3+}-doped δ-$Y_2Si_2O_7$ materials. This study deals with the synthesis and structural and the spectroscopic characterization of the single-phase yttrium disilicate (δ-$Y_2Si_2O_7$) activated with Nd^{3+} ions.

*merdem@marmara.edu.tr; erdemm@bc.edu.
© 2014 The American Ceramic Society

Experimental Study

Nanocrystalline yttrium silicate samples activated with Nd^{3+} were synthesized in the SiO_2–Y_2O_3 binary systems using the solgel method. Precursors with the purity of 99.99% neodymium (III) nitrate hexahydrate ($Nd(NO_3)_3{\cdot}6H_2O$), 99.999% tetraethoxysilane (TEOS, $Si(OC_2H_5)_4$), and 99.9% yttrium nitrate hexahydrate ($Y(NO_3)_3{\cdot}6H_2O$) were used to obtain three different compositions. For all the samples, SiO_2 and Y_2O_3 mole ratios were taken as 7.0 and labeled as NYS_1, NYS_2, NYS_3, and NYS_4, respectively.

The Nd^{3+} concentrations of atoms/cm^3 were calculated using the measured volume and average molecular weight of the each sample by employing the Archimedes principle. The Nd^{3+} concentrations (N_o) were found to be 6.80×10^{19}, 1.02×10^{20}, 1.35×10^{20}, and 1.70×10^{20} atoms/cm^3 for the 0.010, 0.015, 0.020, and 0.025 mol% in the NYS_1, NYS_2, NYS_3, and NYS_4 samples, respectively. Detailed description of the preparation process can be found in our earlier work.[14] The solutions at the final stage were poured into circular Petri dishes and left for 3 weeks at room temperature to obtain the transparent glass samples. The glass samples were then heat treated at 1480°C for 12 h to obtain nanocrystalline δ-$Y_2Si_2O_7$ powders.

The X-ray diffraction (XRD) patterns of the annealed samples were taken by the model Rigaku–XRD D-MAX 2200 with the Cu-Kα source operated with the wavelength at λ = 1.5418 Å. Slit systems, step size (0.02°), source voltage (40 kV), and current (30 mA) were kept constant during the scans that were conducted in θ–2θ coupled mode. The structural and morphological properties of the powders were also investigated by transmission electron microscope (TEM) with model number JEOL JEM-2100.

The continuous emission spectra of the powders were measured by pumping the samples with output of an laser diode (Model S30-808-6) (Apollo Instrument Inc., Irvine, CA) that resulted in the excitation of the levels $^2H_{9/2}$–$^4S_{5/2}$. The luminescence from the powders was directed toward to entrance slit of an action monochromator (Model SP2500) (Acton Princeton Instruments - New Jersey, Trenton, NJ). The optical signal was detected by an InGaAs detector (ID441C) (Acton Princeton Instruments - New Jersey) which uses a thermoelectric cooler. Then, signal was monitored by computer. For further characterization, the responses of the samples to pulsed excitation were obtained using the Schwarz Electro – Optics Inc. Model Titan–P titanium sapphire laser and a Tektronix model TDS3052B oscilloscope (Tektronix, Inc. Beaverton, OR). All measurements were carried out at room temperature.

Results and Discussion

Figure 1 presents the XRD patterns of all nanopowders synthesized by solgel method annealed at 1480°C for 12 h. As the SiO_2–Y_2O_3 phase diagram shows the crystal structures of $Y_2Si_2O_7$ and SiO_2 in the molar region of 67–100% at 1500–1660°C temperature region,[15] the orthorhombic δ-$Y_2Si_2O_7$ (space group $Pna2_1$) and cristobalite SiO_2 phases of the samples without any other phases were identified by comparing the peak positions and intensities with those in the joint commutation powder diffraction standards (JCPDS) in the present study. It was clearly seen that the peak positions correspond well to the standard cards with numbers 45-0043 and 39-1425, respectively.

The average grain sizes and distributions of the powders were estimated from the X-ray patterns using a method based on the two widths at 1/5 and 4/5 of the diffraction line maximum. In this method, the grain sizes obey the gamma distribution function:

$$\mathrm{GSD}(R; R_0, n) = \frac{R_0^{-n-1}}{\Gamma(n+1)} R^n e^{\frac{-R}{R_0}} \tag{1}$$

$$R_0 = \frac{\sigma^2}{<R>}, n = \frac{\sigma^2}{<R>^2} - 1 \tag{2}$$

where R_0 and n are parameters related to the mean grain size $<R>$ and dispersion of the grain size distribution (GSD). More detailed description of the method can be found in.[16] Figure 2 shows the GSD as a function of the grain size. The average grain sizes of the NYS_1,

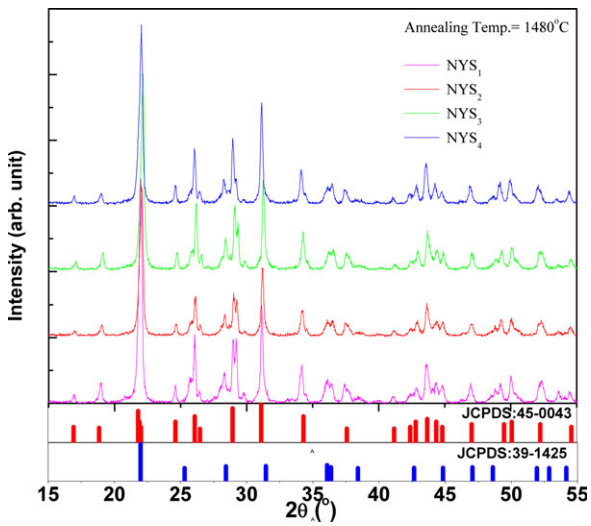

Fig. 1. The X-ray diffraction patterns of all nanopowders synthesized by solgel method annealed at 1480°C for 12 h.

NYS_2, NYS_3, and NYS_4 powders were calculated to be 44.1, 41.3, 48.1, and 53.2 nm from the GSD curves, respectively. The estimated particle sizes were confirmed by TEM micrographs.

The δ-$Y_2Si_2O_7$ crystalline phase is clearly seen from the representative TEM images of NYS_4 powder (see Fig. 3). The inset of the Fig. 3 shows the selected area electron diffraction (SAED) micrograph which points out the crystallinity of the sample. The grains were found to agglomerate with nanosize distribution in all the powders.

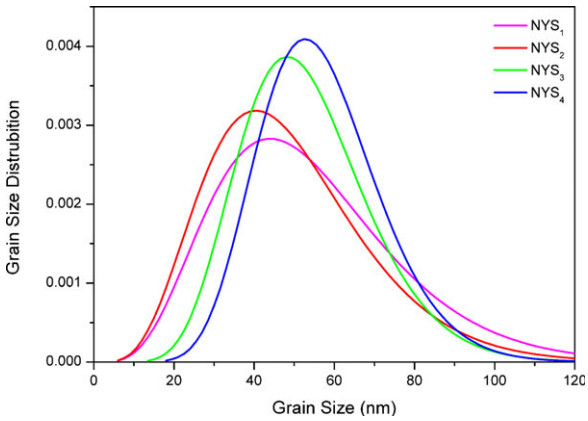

Fig. 2. The grain size distribution of the samples as a function of the grain size.

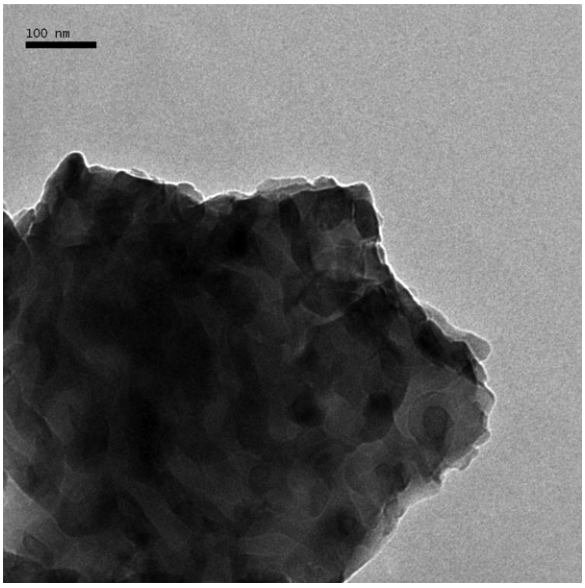

Fig. 3. The transmission electron microscope image of NYS_3 powder.

Figures 4a–c presents the emission spectra of the nanopowders doped with Nd^{3+} ions in the 850–1460 nm wavelength range at 310 K. Each spectrum contains three groups of emission bands centered about 929, 1054, and 1322 nm which are correspond to the transitions from the $^4F_{3/2}$ to $^4I_{13/2}$, $^4I_{11/2}$, and the ground level, ($^4I_{9/2}$) within the 4f shell of the Nd^{3+} ions, respectively. The J-manifolds of Nd^{3+} ions are split due to the low symmetry (C_1 or C_i) [18,17] of the δ-$Y_2Si_2O_7$ cation sites. The spectral profile and the number of the Stark components are the same for each transition of Nd^{3+} ions in the nanopowders. This behavior can be attributed to the fact that the local symmetry of ligand ions surrounding the Nd^{3+} ions is the same for all samples because of the same crystalline phase.[18] In addition, the emission intensity of the lines and bandwidth of the spectral profile for the $^4F_{3/2} \rightarrow {}^4I_{9/2}$, $^4F_{3/2} \rightarrow {}^4I_{11/2}$, $^4F_{3/2} \rightarrow {}^4I_{13/2}$ transitions decrease with increasing Nd^{3+} mole

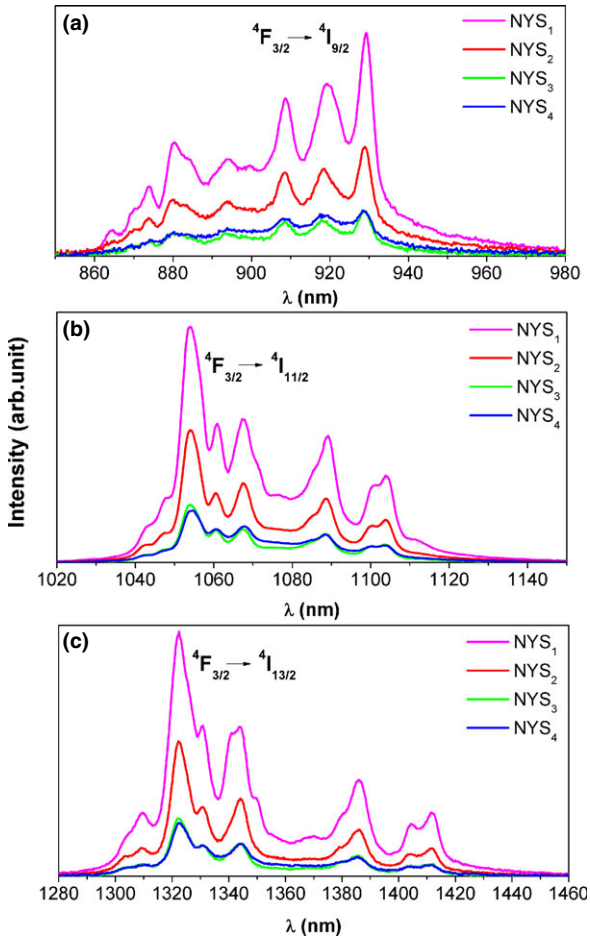

Fig. 4. (a–c) The emission spectra of the nanopowders doped with Nd^{3+} ions in the 850–1460 nm wavelength range at 310 K.

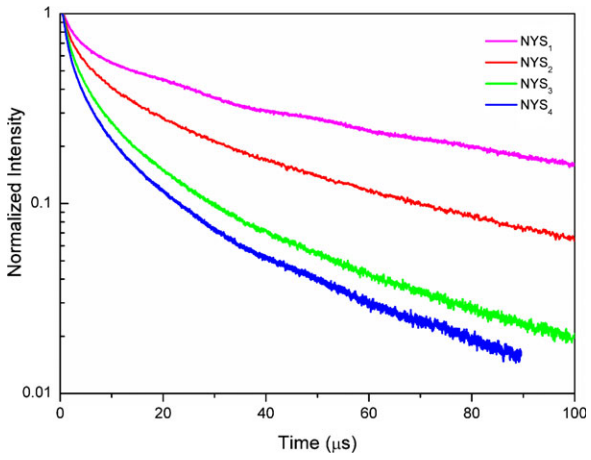

Fig. 5. The decay curves in semi-log scale for all powders.

concentration. The change in intensity with Nd^{3+} concentration may be due to the interaction between the Nd^{3+} ions leading the energy transfer processes.

The decay curves of the $^4F_{3/2}$ level upon the pulsed excitation at 798 nm at room temperature have been measured for all samples. Figure 5 illustrates the decay curves in semi-log scale for all powders. The analyses of these curves led us to conclusions about the effect of crystalline size and Nd^{3+} ion concentration. As seen from Fig. 5, the decay curves of the samples were nonexponential. It is expected to deviate from the exponentiality in nanocrystals. The deviation is due to the increasing surface to volume ratio in nanopowders, the effect of the OH molecular groups residing on the surface, and the existence of interstices between the nanoparticles. As the spontaneous relaxation rates which are the inverse of the radiative lifetime depend on the effective refractive index of the sample, a small change in the sample environment because of existence of these interstices may cause a difference in effective refractive index and as a result change in the radiative lifetimes.[19] Additionally, as seen from Fig. 5, the deviation from the exponentiality between the samples increases with increasing Nd^{3+} ions concentration. This increasing deviation tendency could be due to increasing neighboring Nd^{3+} ions interactions. These Nd–Nd ions interactions are negligible at low dopant concentrations, but they become more dominant at high concentrations. As seen from Fig. 5, the decay time of the $^4F_{3/2}$ emission decreases as the concentration of the Nd^{3+} increases in δ-$Y_2Si_2O_7$ crystalline powders. The faster decay indicates that the effect of concentration quenching started to play an important role with increasing Nd^{3+} ions concentration. This effect might be mainly due to the cross-relaxation of an excited Nd^{3+} ion by giving its energy to a neighboring Nd^{3+} ion.

Conclusions

The δ-$Y_2Si_2O_7$:Nd^{3+} nanocrystalline powders with an average grain size below 53.2 nm were synthesized using the solgel method. The TEM micrographs confirmed the average particle sizes which were calculated using the XRD patterns. The analyses of the decay curves led us to conclusions about the effect of crystalline size and Nd^{3+} ion concentration. However, the effect of the Nd^{3+} concentration on the luminescence properties of the samples has been observed as the decreasing of the luminescence intensity and the shortening of the decay times. The change in the intensities and the decay times with increasing Nd^{3+} ions concentration was attributed to increasing interaction between neighboring dopant ions and as a result increasing concentration quenching effect.

Acknowledgment

This study was financially supported by the Scientific Research Projects Unit (BAPKO) of Marmara University with the project number FEN-B-150513-0170. One of the authors (Murat ERDEM) would like to thank the Scientific and Technological Council of Turkey (TUBITAK) for its support.

References

1. M. Mitsunaga, R. Yano, and N. Uesugi, *Opt. Lett.*, 16 1890–1892 (1991).
2. F. Thibault, D. Pelenc, F. Druon, Y. Zaouter, M. Jacquement, and P. Ana Georges, *Opt. Lett.*, 31 1555–1557 (2006).
3. P. Zhou, X. Yu, L. Yang, S. Yang, and W. Gao, *J. Lumin.*, 124 241–244 (2007).
4. J. Sokolnicki, *Mater. Chem. Phys.*, 131 306–312 (2011).
5. J. Sokolnicki, *J. Lumin.*, 134 600–606 (2013).
6. M. D. Dolan, *et al.*, *Phosphor. Powder Diffr.*, 23 20–25 (2008).
7. J. Felsche, *Struct. Bond.*, 13 99–197 (1973).
8. A. I. Becerro, A. Escudero, P. Florian, D. Massiot, and M. D. Alba, *J. Solid State Chem.*, 177 2783–2789 (2004).
9. M. J. Weber, *J. Non Cryst. Solids*, 123 208–222 (1990).
10. D. S. Funk, J. M. Carlson, and J. G. Eden, *Electron. Lett.*, 30 1859–1860 (1994).
11. A. J. Ferna'ndez-Carrio'n, M. D. Alba, A. Escudero, and A. I. Becerro, *J. Solid State Chem.*,184 1882–1889 (2011).
12. H. W. Dias, F. P. Glasser, R. P. Gunwardane, and R. A. Howie, *Z. Kristallogr.*, 191 117–123 (1990).
13. R. Kaindl, D. M. Tobbens, and V. Kahlenberg, *J. Raman Spectrosc.*, 42 78–85 (2011).
14. M. Erdem, G. Özen, and C. Tav, *J. Eur. Ceram. Soc.*, 31 2629–2631 (2011).
15. J. J. Chambers and G. N. Parsons, *J. Appl. Phys.*, 90 918–933 (2001).
16. R. Pielaszek, *J. Alloy. Compd.*, 382 128–132 (2004).
17. A. A. Kaminskii, *Crystalline Lasers: Physical Processes and Operating Schemes*, CRC Press, New York, NY, 1996.
18. M. Erdem, G. Özen, C. Tav, and B. Di Bartolo, *Ceram. Int.*, 39 6029–6033 (2013).
19. G. Bilir, G. Ozen, J. Collins, and B. Di Bartolo, *Appl. Phys. A*, 115 263–273 (2014).